Journal of Geophysical Research: Space Physics

RESEARCH ARTICLE
10.1029/2017JA025135

Bare Neutron Counter and Neutron Monitor Response to Cosmic Rays During a 1995 Latitude Survey

W. Nuntiyakul[1,2], A. Sáiz[2,3], D. Ruffolo[2,3], P.-S. Mangeard[4,5], P. Evenson[5], J. W. Bieber[5], J. Clem[5], R. Pyle[6], M. L. Duldig[7], and J. E. Humble[7]

[1]Department of Physics and Materials Science, Faculty of Science, Chiang Mai University, Chiang Mai, Thailand, [2]Thailand Center of Excellence in Physics, CHE, Ministry of Education, Bangkok, Thailand, [3]Department of Physics, Faculty of Science, Mahidol University, Bangkok, Thailand, [4]National Astronomical Research Institute of Thailand (NARIT), Chiang Mai, Thailand, [5]Bartol Research Institute, Department of Physics and Astronomy, University of Delaware, Newark, DE, USA, [6]Pyle Consulting Group, Inc., St. Charles, IL, USA, [7]School of Natural Sciences, University of Tasmania, Hobart, Tasmania, Australia

Abstract Neutron monitors of standard design (IGY or NM64) are employed worldwide to study variations in the flux of galactic cosmic rays and solar energetic particles in the GeV range. The design minimizes detector response to neutrons below ~10 MeV produced by cosmic ray interactions in the ambient medium. Increasingly, however, such neutrons are of interest as a means of obtaining spectral information on cosmic rays, for studies of soil moisture, and for nuclear threat detection. Bare neutron counters, a type of lead-free neutron monitor, can detect such neutrons, but comparatively little work has been done to characterize the dependence of their count rate on cutoff rigidity. We analyze data from three bare neutron counters operated on a ship together with a three-tube NM64 monitor from November 1995 to March 1996 over a wide range of magnetic latitude, that is, a latitude survey. The bare counter design used foamed-in-place polyurethane insulation to keep the temperature uniform and to some extent moderate high-energy neutrons. When the ship was near land, the bare/NM64 count rate ratio was dramatically higher. Considering only data from open sea, the bare and NM64 pressure coefficients are not significantly different. We determine the response function of these bare counters, which is weighted to Galactic cosmic rays of lower energy than the NM64. This measurement of the response function may improve determination of the spectral index of solar energetic particles and Galactic cosmic rays from a comparison of bare and NM64 count rates.

Key Points:
- Bare neutron counters and NM64 monitors operated on a ship over a wide range of magnetic latitudes
- Measured bare counter and NM64 response functions are weighted to different Galactic cosmic ray energies
- Bare counter to NM64 count rate ratio relates to spectrum of cosmic rays or solar particles

Supporting Information:
- Supporting Information S1

Correspondence to:
A. Sáiz,
alejandro.sai@mahidol.ac.th

Citation:
Nuntiyakul, W., Sáiz, A., Ruffolo, D., Mangeard, P.-S., Evenson, P., Bieber, J. W., et al. (2018). Bare neutron counter and neutron monitor response to cosmic rays during a 1995 latitude survey. *Journal of Geophysical Research: Space Physics*, *123*, 7181–7195. https://doi.org/10.1029/2017JA025135

Received 18 DEC 2017
Accepted 10 AUG 2018
Accepted article online 20 AUG 2018
Published online 8 SEP 2018

1. Introduction

Neutron monitors are ground-level detectors of cosmic-ray-induced atmospheric secondary particles that respond mostly to secondary neutrons (Simpson, 1948). Neutron monitors of the standard IGY and NM64 designs are optimized so that their count rates provide a precise and reliable measurement of the GeV-range cosmic-ray flux (Hatton & Carmichael, 1964). In particular, a neutron monitor at a given location is most sensitive to cosmic rays within a range in rigidity (momentum per charge, expressed in GV) somewhat above the local geomagnetic cutoff, which varies from near 0 GV at Earth's polar regions to ~17 GV at some parts of the geomagnetic equator, and above the atmospheric cutoff of $\gtrsim$1 GV needed to generate atmospheric secondary particles that can be recorded at ground level (see the response functions determined by Nuntiyakul et al., 2014). A standard neutron monitor includes a *producer*, typically ~5–30 tons of lead, in which atmospheric secondary particles of $\geq$10 MeV have a high probability of interacting to produce multiple MeV-range neutrons that can be detected in gas-filled proportional counters containing ^{10}B or ^{3}He. A standard neutron monitor is also surrounded by a *reflector* comprising several centimeters of paraffin or polyethylene, which aims to contain the neutrons produced in the lead as well as minimize the detector response to secondary neutrons of $\leq$10 MeV, which are mainly produced by cosmic ray interactions in surrounding materials at ground level and thus are sensitive to changes in the local environment. Also important is the *moderator*, consisting typically of a thinner layer of the same material as the reflector placed between the lead producer and each gas-filled counter, which helps slow down the neutrons in order to be detected efficiently. Standard neutron monitors are operated at more than 40 locations worldwide, taking advantage of the varying geomagnetic cutoff, and are widely used to monitor Earth's radiation environment due to relativistic solar energetic

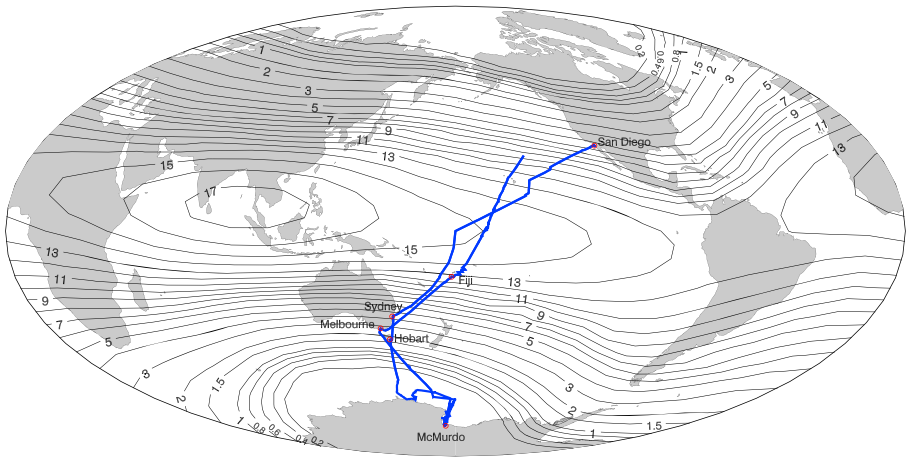

Figure 1. Track of the USCGC Polar Star for the 1995–1996 survey, superimposed on contours of vertical cutoff rigidity. Numbers give vertical cutoff rigidity in GV. This survey carried a standard neutron monitor (3NM64) and three bare neutron detectors, permitting a direct comparison of their response to primary cosmic rays.

particles and galactic cosmic rays and their variations associated with solar activity, and for applications concerning space weather and space radiation.

Such observations can be complemented by measurements using bare neutron counters that lack the reflector and lead producer of standard neutron monitors, making them also sensitive to atmospheric neutrons of $\leq$10 MeV. Such detectors are widely used to detect soil moisture (Zreda et al., 2008), for nuclear threat detection (Kouzes et al., 2008), and to obtain spectral information on solar energetic particles.

From a fixed location, a standard neutron monitor (NM64) count rate alone cannot be used to measure the energy spectrum of cosmic rays. However, since a bare counter (BC) has a different energy response from an NM64, operating them together provides some knowledge of the spectrum (e.g., Bieber & Evenson, 1991; Bieber et al., 2013) while avoiding the systematic errors of comparing count rates from different locations (Figure 2 of Ruffolo et al., 2016). The accuracy of this method requires knowing how the energy responses of the different types of detector are related.

In this work we focus on developing optimal methods for extracting the response function of three BCs that were operated aboard the U.S. Coast Guard icebreaker *Polar Star* along the route illustrated in Figure 1. This voyage was one of a series of latitude surveys in which the magnetic field of the Earth was used as a spectrometer to explore the time dependence of the spectrum of cosmic rays striking the atmosphere (Nuntiyakul et al., 2014). All of these surveys carried a NM64 neutron monitor with three counter tubes, that is, a 3NM64, and in addition the survey from San Diego, USA, to McMurdo, Antarctica, and back during a voyage of ~4 months from 6 November 1995 to 20 March 1996 carried three bare detectors. To our knowledge, there have been two previously published bare surveys: the 1976 survey (Stoker et al., 1980) did not extend to polar latitudes, and the 1996 survey (Dorman et al., 2000; Villoresi et al., 2000) was conducted with unmoderated bare detectors. Therefore, direct comparison of results is difficult.

2. Methodology

2.1. Latitude Surveys and Response Functions

The count rate $N(t)$ of a ground based detector resulting from the impact of cosmic rays at the top of the atmosphere is described by

$$N(\Theta,\Phi,h,t) = \int_0^\infty \left[\sum_i J_i(P,t)\, Y_i(P,h)\right] T(P,\Theta,\Phi,t)\, \mathrm{d}P, \tag{1}$$

where J_i is the Galactic cosmic ray spectrum for primary cosmic rays of particle type i near Earth expressed as a function of rigidity (P) and time (t). The primary cosmic rays are approximately 90% protons (in particle number) while 9% are alpha particles (helium nuclei) and 1% are the nuclei of heavier elements; their fluxes near Earth include variations with the 22-year solar magnetic and 11-year solar activity cycles as the result of

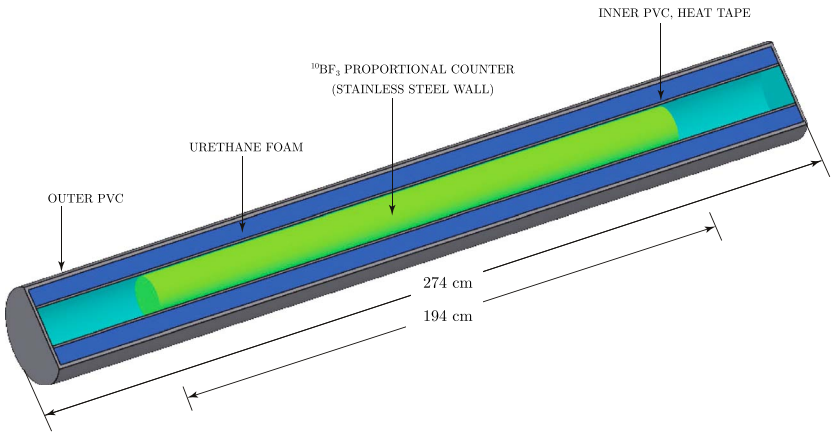

Figure 2. Rendered sketch of the "bare" neutron counter configuration used in this work. Each BP-28 neutron-sensitive proportional counter was operated inside a 20-cm-diameter PVC pipe covered with heat tape and thermally insulated by foamed-in-place polyurethane inside a larger, 30 cm diameter PVC pipe. Three such bare counters and a three-counter neutron monitor were operated along the survey route shown in Figure 1.

interactions with the solar wind and magnetic fields in interplanetary space. (Here we neglect the cosmic ray anisotropy, which is usually $\lesssim 1\%$.) The yield function Y_i for primary particles of type i, a function of rigidity (P) and atmospheric depth (h), is the actual relationship between the cosmic ray flux at the top of atmosphere and the observed count rate from the detectors. The transmission function T_i describes the transmission through the magnetosphere of the Earth. It is a function of particle rigidity (P), latitude (Θ) and longitude (Φ) of the detector location, and time (t).

At a given latitude and longitude, the effective cutoff rigidity for transmission through Earth's magnetic field depends on the arrival direction of each primary cosmic ray described by the local zenith and azimuthal angles. However T_i can be approximated by a step function at a single cutoff rigidity P_c, that we call the *apparent cutoff rigidity*. With the assumption that the transmission is a step function, the count rate relation becomes

$$N(P_c, h, t) = \int_{P_c}^{\infty} \sum_i J_i(P, t)\, Y_i(P, h)\, \mathrm{d}P. \tag{2}$$

The apparent cutoff used in this work considers both vertically incident particles and obliquely incident particles (Clem et al., 1997); this is calculated individually at 1-hr intervals at the actual position of the ship with a time-dependent model of the magnetic field according to an *efficient* method (Bieber et al., 1997). We use a particle propagation code from the Bartol Research Institute (Lin et al., 1995) together with an accurate model of the terrestrial magnetic field including any field disturbance present as indicated by the K_p index value at the time. K_p quantifies variations of the horizontal component of the magnetic field of the Earth as an integer in the range 0–9, that is, a lower number indicates quiet conditions and a higher number indicates a stronger geomagnetic storm (Thomsen, 2004).

The differential response function (DRF) is defined as the negative of the derivative of the count rate as a function of cutoff rigidity. The most common type of analysis for measuring a response function is the Dorman et al. (1969) analysis, in which corrections are first applied to the data points, then a parameterized function of apparent geomagnetic cutoff rigidity, termed a *Dorman function*, is fitted to the data:

$$N(P_c) = N_0 \left(1 - \mathrm{e}^{-\alpha P_c^{-\kappa}}\right), \tag{3}$$

where N_0, α, and κ are unphysical parameters that provide a good representation of the integral response function N, which can be analytically differentiated to determine the DRF:

$$N(P_c) = \int_{P_c}^{\infty} \mathrm{DRF}\,(P)\, \mathrm{d}P, \tag{4}$$

$$\mathrm{DRF}\,(P) = N_0 \alpha P^{-\kappa-1} \kappa\, \mathrm{e}^{-\alpha P^{-\kappa}}. \tag{5}$$

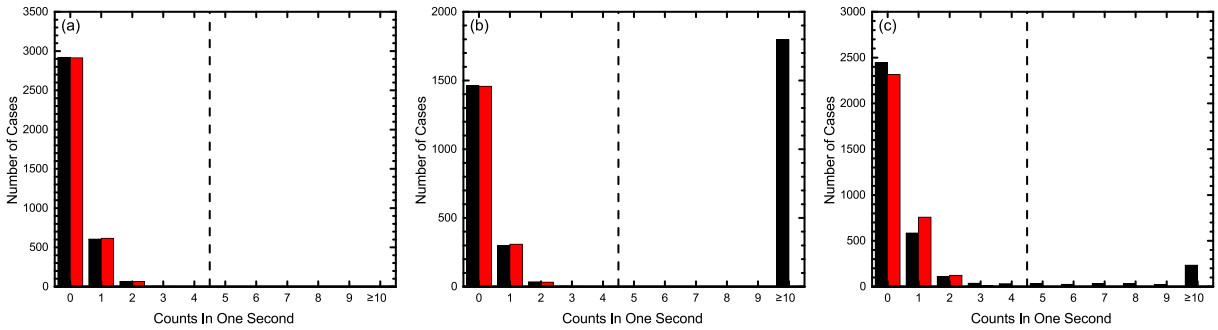

Figure 3. Examples of 1-s count distributions (black) and Poisson distributions based on the rates of 0–4 counts (red), each for 1 hr from one bare counter. (a) This measured distribution closely matches a Poisson distribution. (b) Here many seconds had multiple counts, but the distribution of 0–4 counts closely matches a Poisson distribution. (c) Ambiguous data. In all cases only the data to the left of the dashed line were used in further analysis.

From equations (2) and (4), we can express the DRF as the summed product of $J_i(P, t)$ and $Y_i(P, h)$:

$$\text{DRF}\,(P) = -\left[\frac{dN}{dP_c}\right]_P = \sum_i J_i(P, t)\, Y_i(P, h). \tag{6}$$

2.2. Instrumentation

The 1995 latitude survey employed two types of neutron detectors, three bare neutron detectors and a 3NM64 neutron monitor. The three BCs were installed exposed on an upper deck of the ship, whereas the 3NM64 was installed in an insulated shipping container (called the "TasVan"). Nuntiyakul et al. (2014) provide a detailed description of the TasVan and the series of latitude surveys. In summary, the detectors are Chalk River BP-28 proportional counter cylinders filled with boron trifluoride gas (enriched in the isotope ^{10}B). The boron nuclei react with neutrons and undergo nuclear fission. The reaction products (^{4}He and ^{7}Li) ionize the gas and eventually produce electrical pulses on a central anode wire maintained at ground, while a cylindrical outer cathode is at a potential of about −2,800 V.

Unlike for an NM64, there is no standard design for a bare neutron counter. The detectors discussed in the present work were prototypes for a system that was intended for outdoor deployment at the South Pole. The design used 2-lb density (2 lb/ft^3 ∼ 32 kg/m^3) foamed-in-place polyurethane insulation for thermal control between an inner, 8" thin-wall PVC pipe (outer diameter 219 mm, thickness 4.75 mm) and an outer, 12" schedule-40 PVC pipe (outer diameter 324 mm, thickness 10.3 mm), which also served as a moderator for high-energy secondary neutrons. The standard polyethylene moderator on a BP-28 was not used. A rendered drawing of the detector is shown in Figure 2.

3. Data Reduction

3.1. Overview

Throughout this work all the dates during the survey will be referred to as "day of the year of 1995" (DOY1995). The 12th generation International Geomagnetic Reference Field (IGRF12) and the 1989 revision of the Tsyganenko (1987) model were used for calculating the cutoff rigidity. Numerical results for the 3NM64 in the present work differ slightly from those presented by Nuntiyakul et al. (2014) for three main reasons: (1) data intervals were selected such that they had good data in both the BCs and the 3NM64 whereas the earlier study only considered the 3NM64; (2) no corrections for short term modulation based on the McMurdo count rate were applied in this work; and (3) no normalization of the data to the McMurdo count rate was performed in this work.

3.2. Initial Processing

The most serious problem encountered in the data was mutual interference of the instrument with communications equipment on the ship. This equipment was used only when at sea, so any attempt at debugging the problems during port calls was not possible. However, a relatively simple realization enabled the extraction of a useful data set. Our data were recorded with one second time resolution together with clinometer readings to allow for possible corrections due to the varying orientation of the ship in rough seas. Looking closely at the 1-s data, we found that the noise was often quite "bursty" with seemingly unaffected seconds interspersed with seconds recording hundreds of counts.

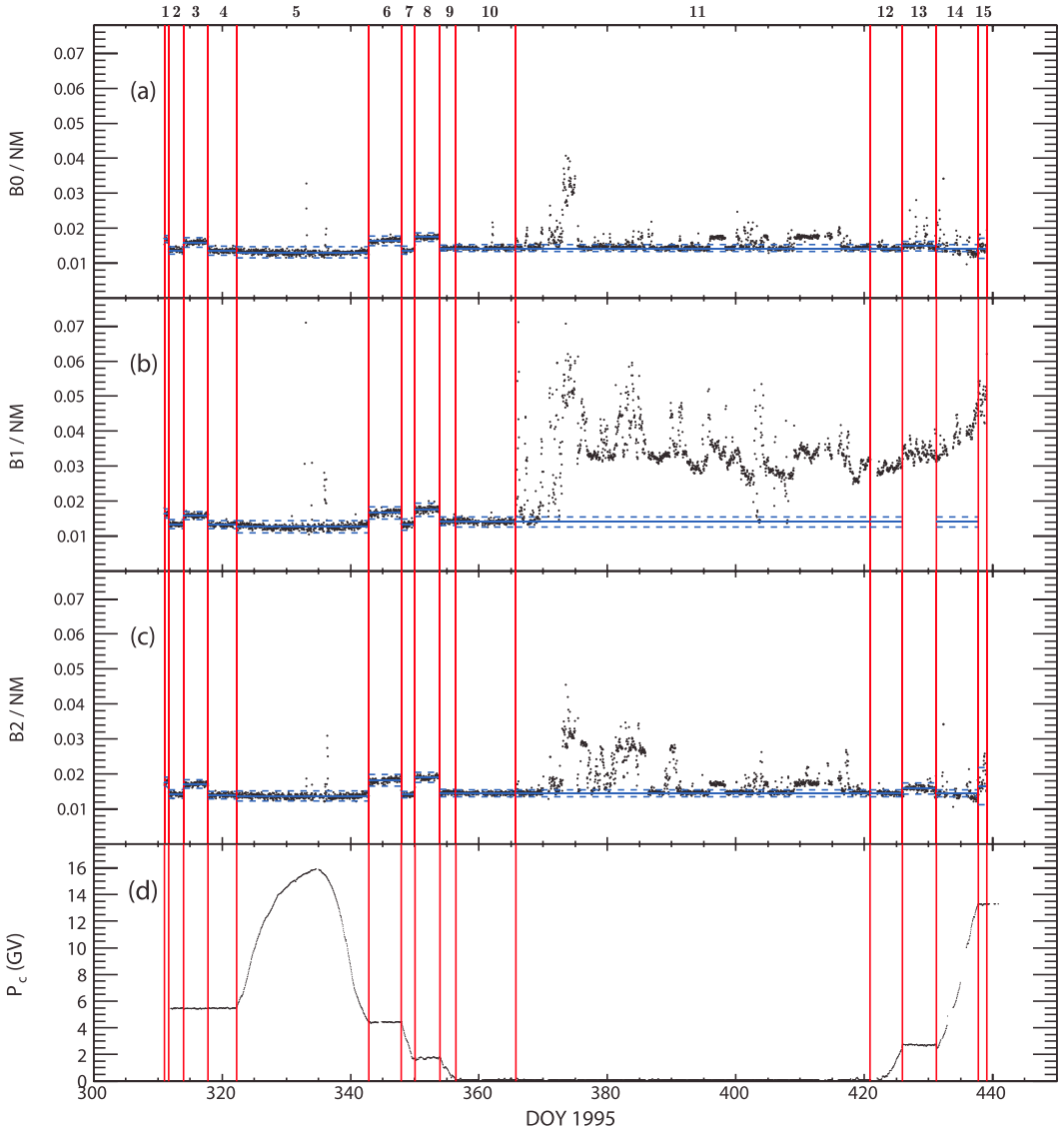

Figure 4. Summary of hourly averaged data as a function of time. (a)–(c) Ratios of individual bare detector count rates to 3NM64 count rate. Red vertical lines define 15 time periods used in the analysis. In each time period, the horizontal blue solid line shows the reference value $\langle B_i/\mathrm{NM}\rangle$ and blue dashed lines illustrate the $\pm 3\sigma$ interval around the reference. (d) Apparent geomagnetic cutoff rigidity P_c.

We therefore made histograms of the 1-s readings for each tube for each hour of the survey, with typical examples shown in Figure 3. The observed distribution of counts is shown in black whereas the red shows the Poisson distribution expected based on the average rate over the first five channels. Figure 3a shows an hour with essentially no noise—typical of all of the time spent in port when the investigators had access to the equipment. In this case all of the individual measurements fall nicely on the distribution. Figure 3b shows a case where there is a clean Poisson component plus a clearly separated noise component. In Figure 3c the separation fails, for reasons that we have been unable to establish. We investigated automatically extracting data from noisy hours based on a quantitative test for deviations from a Poisson distribution in the first five channels but no clear method emerged. Instead, we prepared our basic data set with 1-hr resolution by taking averages over the first five channels (those left of the dashed lines) independent of the quality of fit to a Poisson distribution. We deferred rejecting bad hours to a later stage of analysis.

The data set thus obtained is plotted in Figure 4. In this figure we show hourly averages of BC count rates divided by NM count rates (where NM means the summed count rate of the three counters in the 3NM64), without any further correction. On this plotting scale the small variations in the ratios due to cutoff variation

Table 1
Reference BC to NM Count Rate Ratios

Period	Start DOY	Environment	$\langle B_0/\mathrm{NM}\rangle \pm \sigma$	$\langle B_1/\mathrm{NM}\rangle \pm \sigma$	$\langle B_2/\mathrm{NM}\rangle \pm \sigma$
TP1	311.000	San Diego	0.0169 ± 0.0003	0.0165 ± 0.0004	0.0177 ± 0.0005
TP2	311.667	Naval maneuvers	0.0137 ± 0.0004	0.0134 ± 0.0004	0.0142 ± 0.0004
TP3	314.000	San Diego	0.0159 ± 0.0004	0.0159 ± 0.0004	0.0171 ± 0.0004
TP4	317.833	Naval maneuvers	0.0136 ± 0.0004	0.0133 ± 0.0004	0.0139 ± 0.0003
TP5	322.250	Open sea	0.0131 ± 0.0005	0.0127 ± 0.0006	0.0137 ± 0.0005
TP6	342.875	Sydney	0.0164 ± 0.0005	0.0166 ± 0.0006	0.0181 ± 0.0005
TP7	347.917	Open sea	0.0137 ± 0.0004	0.0133 ± 0.0005	0.0140 ± 0.0003
TP8	350.042	Hobart	0.0174 ± 0.0004	0.0176 ± 0.0006	0.0190 ± 0.0005
TP9	353.917	Open sea	0.0143 ± 0.0003	0.0143 ± 0.0004	0.0145 ± 0.0004
TP10	356.375	Open sea	0.0143 ± 0.0003	0.0141 ± 0.0005	0.0145 ± 0.0003
TP11[a]	365.792	Mixed	0.0143 ± 0.0003	0.0141 ± 0.0005	0.0145 ± 0.0003
TP12[a]	420.917	Open sea	0.0143 ± 0.0003	0.0141 ± 0.0005	0.0145 ± 0.0003
TP13	425.917	Melbourne	0.0149 ± 0.0004	—	0.0158 ± 0.0006
TP14[a]	431.208	Open sea	0.0143 ± 0.0003	0.0141 ± 0.0005	0.0145 ± 0.0003
TP15	437.792	Fiji	0.0142 ± 0.0010	—	0.0166 ± 0.0018

[a]Using reference values measured for TP10.

are not readily visible. We term the count rates of the three BCs as B_0 for the left BC, B_1 for the center BC, and B_2 for the right BC. The reference values are explained in the following section. The figure also shows the calculated apparent cutoff rigidity as a function of time.

The shown data set, which includes the correction for instrumental interference explained above, still contains many clear outliers with a count rate enhanced beyond 3σ above the reference value, especially for the center BC after DOY 370. For those outlier hours with high hourly average count rates, the counts-per-second distributions show no recognizable noise component or signatures of double pulsing, so we conjecture that some change in the surroundings may have caused the neutron flux to be enhanced (possibly materials stored in the space immediately under the detectors). In any case, only data within $\pm 3\sigma$ of the reference value are selected for further analysis, as specified below.

Table 2
Reference BC to BC Count Rate Ratios

Period	Start DOY	Status	$\langle B_0/B_1\rangle \pm \sigma$	$\langle B_1/B_2\rangle \pm \sigma$	$\langle B_2/B_0\rangle \pm \sigma$
TP1	311.000	San Diego	1.015 ± 0.03	0.933 ± 0.04	1.053 ± 0.04
TP2	311.667	Naval maneuvers	1.032 ± 0.04	0.939 ± 0.03	1.033 ± 0.03
TP3	314.000	San Diego	1.001 ± 0.03	0.926 ± 0.03	1.075 ± 0.04
TP4	317.833	Naval maneuvers	1.028 ± 0.04	0.947 ± 0.03	1.030 ± 0.04
TP5	322.250	Open sea	1.034 ± 0.06	0.927 ± 0.05	1.045 ± 0.05
TP6	342.875	Sydney	0.987 ± 0.04	0.916 ± 0.03	1.106 ± 0.04
TP7	347.917	Open sea	1.027 ± 0.05	0.957 ± 0.04	1.026 ± 0.04
TP8	350.042	Hobart	0.991 ± 0.04	0.926 ± 0.04	1.090 ± 0.03
TP9	353.917	Open sea	1.008 ± 0.04	0.975 ± 0.03	1.018 ± 0.03
TP10	356.375	Open sea	1.018 ± 0.03	0.976 ± 0.04	1.013 ± 0.03
TP11[a]	365.792	Mixed	1.018 ± 0.03	0.976 ± 0.04	1.013 ± 0.03
TP12[a]	420.917	Open sea	1.018 ± 0.03	0.976 ± 0.04	1.013 ± 0.03
TP13	425.917	Melbourne	—	—	—
TP14[a]	431.208	Open sea	1.018 ± 0.03	0.976 ± 0.04	1.013 ± 0.03
TP15	437.792	Fiji	—	—	—

[a]Using reference values measured for TP10.

Table 3
Pressure Coefficient of BC to NM Count Rate Ratios for Fixed Stations

Location	Epoch	Altitude (m)	P_c (GV)	b (10^{-4} mmHg^{-1})	BC rate[a](s^{-1})	NM rate[a](s^{-1})	Ratio
Doi Inthanon	2007–2013	2560	17.4	3.30 ± 0.49	6.0	34.0	0.176
Newark	2015–2016	40	2.3	9.13 ± 0.06	2.7	12.0	0.225
McMurdo	2016	48	< 0.1	2.16 ± 0.09	3.2	16.7	0.192
South Pole, BF_3	1990–2004	2820	< 0.1	4.10 ± 0.16	15.0	87.0	0.172
South Pole, ^{3}He	2005–2016	2820	< 0.1	2.94 ± 0.07	12.5	103.0	0.121

[a]Average rates per tube.

3.3. Data Cleaning Based on Neutron Monitor Count Rate

The selection of usable data (data *cleaning*) and the adjustment of bad or missing individual counter data (data *correction*) are performed based on BC-to-NM ratios (B_i/NM) and BC-to-BC ratios (B_i/B_j).

We start by choosing appropriate time periods during the 1995 survey year for which data were taken in a relatively stable environment. The 15 time periods used (TP1 to TP15) are indicated in Tables 1 and 2, and shown in Figure 4. Data cleaning is then applied separately for each time period. This division into time intervals is based on the locations near which the ship passed, that is, San Diego, Sydney, Hobart, McMurdo, Melbourne, and Fiji, as well as on apparent step-like changes in the ratio values elsewhere.

For each time period we generated histograms of the hourly B_i/NM values to characterize and remove outliers. Figures 4a–4c illustrate the individual B_i/NM ratios as a function of time. The red vertical lines show the division in time periods. The blue solid horizontal lines illustrate the B_i/NM *reference values* $\langle B_0/\mathrm{NM}\rangle$, $\langle B_1/\mathrm{NM}\rangle$, and $\langle B_2/\mathrm{NM}\rangle$. In most cases, these were defined as the mean of a Gaussian fit to the ratio histogram for each time period. For three time periods, namely TP11, TP12, and TP14, we used the reference calculated during TP10 because it was noticed that the noise was too high for the center BC (B_1). Using the TP10 ratio reference for those three problematic time periods, we avoided bias in the data that could induce further analysis errors. For the $\langle B_1/\mathrm{NM}\rangle$ ratio reference, during TP13 and TP15 data were also noisy but no appropriate reference based on another time period with similar environment could be identified, so those intervals have no reference available. The blue horizontal dashed lines illustrate plus and minus three standard deviations from the reference for each time period, also based on the Gaussian fit. The $\langle B_i/\mathrm{NM}\rangle$ ratio reference values and their standard deviations σ for the 15 time periods are also shown in Table 1. B_i/NM data points lying outside the range defined by 3 standard deviations (i.e., $\pm 3\sigma$) from the reference were considered to indicate bad data and the count rate B_i was then corrected (if possible) as explained in the next section or removed before subsequent analysis.

3.4. Data Correction Based on BC Ratios

The rough and changing conditions on board the ships caused the response of individual BCs to occasionally change, become noisy, or even stop completely. In order to correct for these effects during the surveys, we used the inherent redundancy of the three bare detectors.

The histograms of individual BC ratio values (B_0/B_1, B_1/B_2, and B_2/B_0) were plotted for each time period (except for periods with no appropriate reference for the B_i/NM ratio, as mentioned above). For TP1–TP10, reference values were calculated for these BC ratios based on a fit to a Gaussian, but for TP11, TP12, and TP14 we used the BC ratio reference of TP10 instead. For TP13 and TP15, the BC ratios were not used because the center tube had bad counts during the whole time period and there was no other appropriate reference.

The BC ratio references $\langle B_0/B_1\rangle$, $\langle B_1/B_2\rangle$, and $\langle B_2/B_0\rangle$ and their standard deviations for the 15 time periods are shown in Table 2. We defined the range of three standard deviations ($\pm 3\sigma$) from the reference values $\langle B_i/B_j\rangle$ to select good data points (count rates B_i and B_j that needed no further correction) or identify count rates that needed to be corrected. The reference values for the BC ratios were then used to correct those count rates, using the same method as explained in Nuntiyakul et al. (2014). The count rates of the three bare tubes for each hour (B_1, B_2, and B_3) were corrected if the BC ratio data were outside the 3σ range and there was a valid BC ratio reference for calculating the missing data. We calculated a corrected count rate from the actual count rate of the properly operating detectors. If only one tube was ignored, we calculated the corrected count rate based on the measurement in the other two tubes and the ratio reference values. If two tubes were

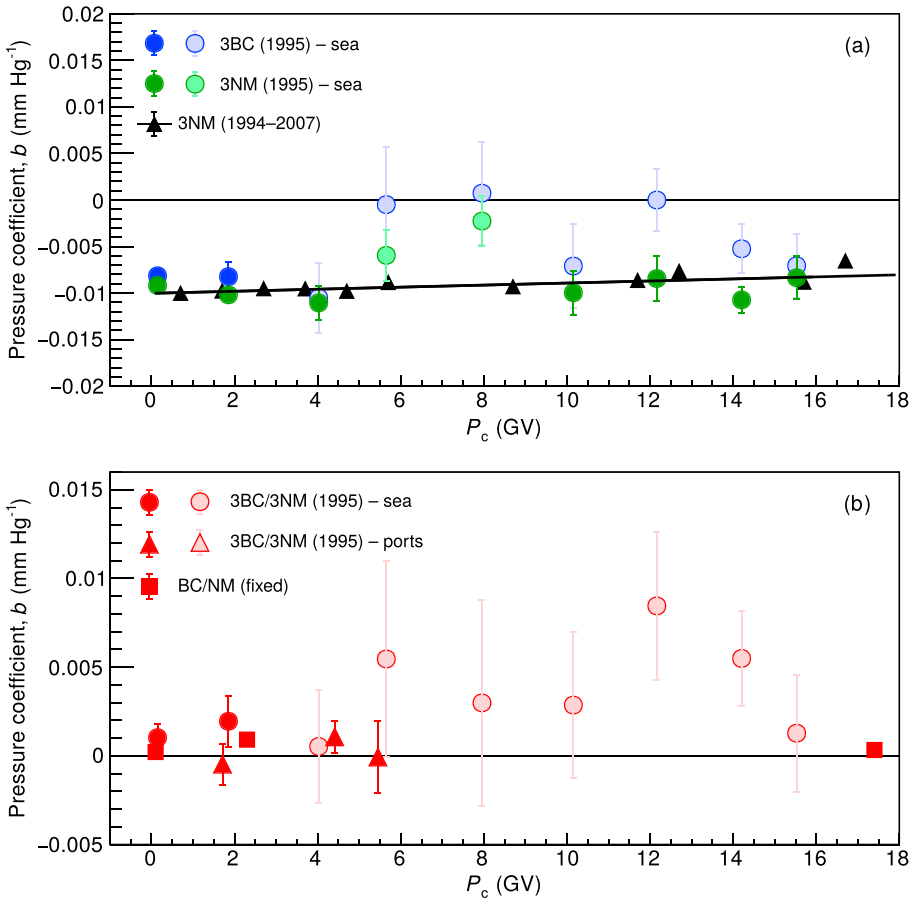

Figure 5. Pressure coefficient *b* (defined in text) as a function of apparent geomagnetic cutoff rigidity P_c. (a) Black triangles and heavy line: 3NM64 from 13 years of summed data (Nuntiyakul et al., 2014). Green circles: 3NM64 from 1995 data. Blue circles: three bare counters (3BC) from 1995 data. (b) Red circles: 3BC/3NM64 ratio in 1995, open sea. Red triangles: 3BC/3NM64 ratio in 1995, near land. Red squares: Fixed locations. Pastel shaded points are less accurate, with standard errors of *b* larger than 0.0025 $mmHg^{-1}$.

removed, we similarly used the remaining tube to determine the corrected count rates. If none of the tubes were operating properly, that hour was considered a data gap.

3.5. Barometric Pressure Correction

Although Stoker and Raubenheimer (1985) report that there is no difference between the barometric pressure correction coefficient for BCs and NM64, they have been measured to be different for the neutron monitor at Doi Inthanon, Thailand (Muangha, 2013). The first entry in Table 3 gives the result of that analysis. As the correction for variation in barometric pressure is critical to proper interpretation of the data, we carefully investigated this with the data from the 1995 survey.

We define a pressure coefficient (*b*) as the slope of a linear fit to the logarithm of counting rate as a function of barometric pressure. To control for short term variations, we extract this by calculating the deviation of the hourly average of each quantity from the overall average for that day.

We determined *b* separately for the 3NM64 and the BCs, with the data divided into bins of apparent cutoff rigidity. The width of each bin was determined by the number of data points available. Results of this analysis are shown in Figure 5a, along with the more statistically accurate determinations based on 13 years of data in Nuntiyakul et al. (2014). We also calculated pressure coefficients for the ratios of the summed count rate of the three BCs (3BC) to that of the 3NM64. Since there is no evidence for a major difference in coefficients from the survey data alone, in the present analysis we have corrected both 3BC and 3NM64 with the well-determined coefficient from the 13-year data set for the 3NM64.

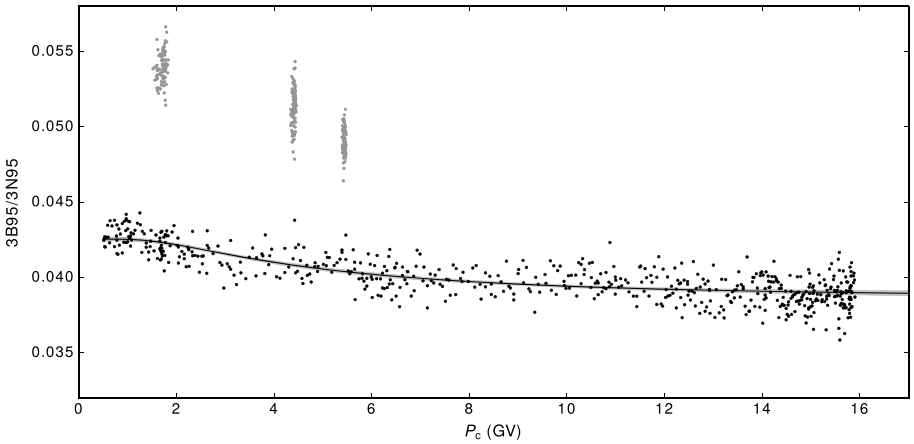

Figure 6. BC/NM ratio in 1995 as a function of apparent geomagnetic cutoff rigidity P_c. Black dots: ship in open sea. Gray dots: port calls at Hobart (P_c = 1.71 GV), Sydney (P_c = 4.41 GV), and San Diego (P_c = 5.45 GV). Line: ratio of Dorman functions shown in Figures 7a and 7b. Each dot represents a 1-hr data point.

We also extracted coefficients from historical data for two different land-based BC configurations and the 3 × 1NM64 neutron monitor at South Pole and for BCs and an 18NM64 at Doi Inthanon, Thailand. In addition, we set up BCs at Newark, Delaware (three spare BP-28 counters) and McMurdo (one BP-28 removed from the NM64) to investigate this issue. Results are plotted in Figure 5b and given in detail in Table 3, along with various parameters characterizing the stations. Here *b* refers to the pressure coefficient of the ratio of the BC and NM64 count rates per tube, which corresponds to the difference in pressure coefficients of the two types of neutron detectors. All of the land-based installations show small positive coefficients. The value at Newark is significantly larger than those at South Pole, McMurdo, and Doi Inthanon. The building construction (masonry with slate roof) at Newark is different from the light construction at the other stations. In general, there is no specific pattern with altitude or cutoff; rather the data provide an additional caution regarding the environmental sensitivity of bare detectors. In other words, the observed pressure coefficient of the shipborne BC to NM64 count rate ratio is consistent with zero, given the uncertainties.

3.6. Temperature Correction

We investigated the need for a temperature correction. The BCs were in a different location from the three neutron monitors and neither had very good temperature control. We know from Evenson et al. (2005) that temperature correction coefficients are different for NM64s operated with $^{10}BF_3$ and ^3He detectors. Therefore we looked for temperature effects by searching for correlations of the measured ratios with differences in the measured tube temperatures. Within the statistical accuracy permitted by the data, we could not find any. Therefore we did not attempt a temperature correction for the present study.

3.7. Port Effects

The extreme sensitivity of bare detectors to the environment is clearly illustrated in Figure 6, which shows the ratio of the BC to NM count rate after all of the corrections discussed above have been applied. Substantial increases in the ratio occur whenever the ship is in port, as was also found by Villoresi et al. (2000). This can be explained by a higher density of albedo neutrons near solid ground compared with open water, and the fact that neutron detectors lacking a reflector (such as the BCs) are much more sensitive to these environmental neutrons than the standard NM64. We therefore classified the data carefully so as to be certain that the results we report are representative of the open ocean. Times "near port" were defined to be when the ship was close to port and "ocean" times were when the ship was away from land. This consideration was used when establishing the 15 time periods as shown in Figure 4 divided by red vertical lines. As noted above, the BC/NM ratio was high near ports but lower when the ship was at sea. For example, around San Diego (P_c = 5.45 GV, TP1 and TP3) the ship moved to near port twice, once at Sydney (P_c = 4.41 GV, TP6), and once at Hobart (P_c = 1.71 GV, TP8). Data from port calls near McMurdo (two steps in TP11), Melbourne (TP13), and Fiji (TP15) are not included in our analysis, according to the procedure described in section 3.4, because they had no ratio reference to clean the data.

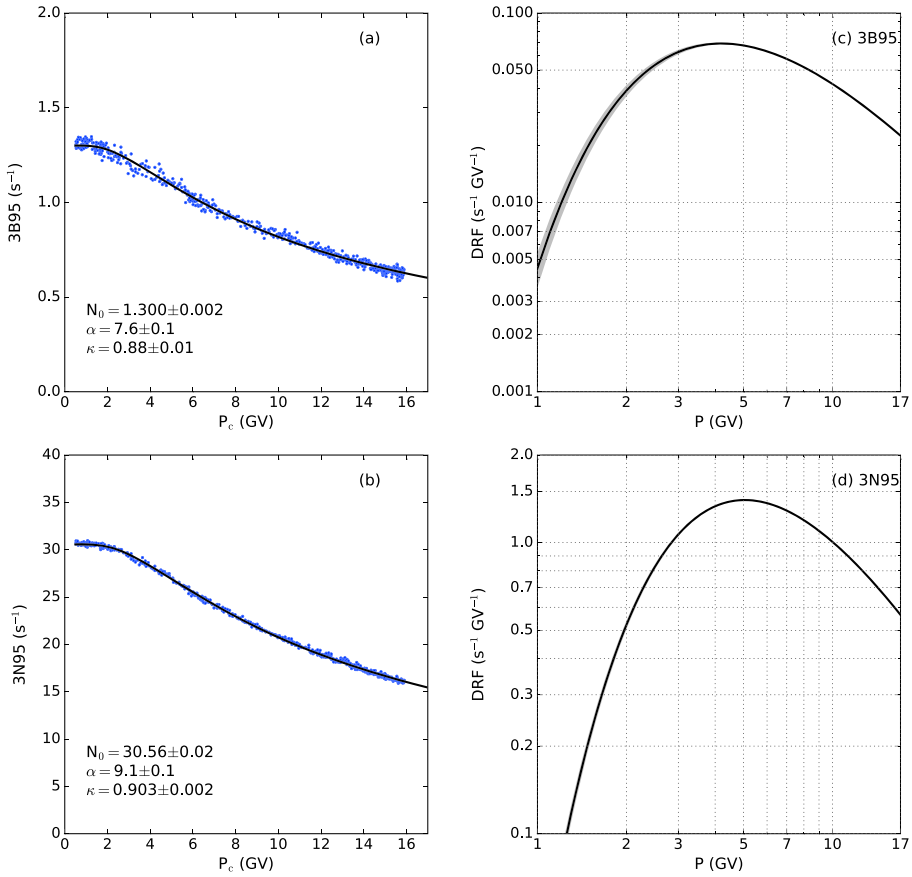

Figure 7. Dorman function fits to (a) bare and (b) neutron monitor data separately; (c) and (d) show the resulting differential response functions (DRFs).

4. Discussion

4.1. 1995 Survey

To quantify the dependence shown in Figure 6 we performed a fit to a Dorman function (Dorman et al., 1969) to the data for 3BC and 3NM64 separately. To do the fit we minimize the least squares function using the Levenburg-Marquardt algorithm and provide estimates for the statistical errors in the determination of the parameters from the scatter of the data points about the resulting fit. The results of the fits are shown in Figure 7. In this case, as in subsequent ones, we show the best fit as a solid line and the (two sigma) range of possible fits as a shaded area. In many cases the shaded area cannot be distinguished from the solid line. The parameters of these fits, along with other Dorman fit parameters discussed later, are summarized in Table 4. This Table also defines the nomenclature used in further discussions of these fits. The present analysis of the 3NM64 count rate from the 1995 survey differs from that of Nuntiyakul et al. (2014) for the same survey in that the present data are restricted to time periods with usable BC data, without correction for short-term cosmic ray variations and without a normalization factor of 1.015 to account for the 3NM64 location on the ship relative to other survey years.

DRFs, as well as the fit parameters, depend on the physical size of the detectors. To compare the inherent response of the 3BC and 3NM64, some normalization is necessary. Various normalizations are proposed in the literature, but for our purposes we adopt a rather simple one, namely, setting the parameter N_0 to one. This corresponds to normalizing the counting rate of a detector to 1.0 at zero cutoff. With this normalization we compare our DRF for the BCs to that for monitors in Figure 8. As expected, the response of the BCs is significantly greater than that of the monitors at low rigidity.

4.2. Comparison with 1976 and 1996 Surveys

Figure 9 compares our results with various interpretations of the data from the 1976 survey (Stoker et al., 1980) and the 1996 survey (Dorman et al., 2000). The 1995 and 1976 surveys were performed under remarkably sim-

Table 4
Dorman Function Fit Parameters

Configuration	Analysis	Survey year	Tag	N_0 (s^{-1})[a]	α	κ
3NM64	This Work	1995	3N95	30.56(2)	9.1(1)	0.903(2)
3NM64	Nuntiyakul et al. (2014)	1995	—	30.9	9.05	0.899
3BC	This Work	1995	3B95	1.300(2)	7.6(1)	0.88(1)
1BC	Stoker (1985) (A)	1976	1B76A	157.68[b]	7.32	0.898
1BC	Stoker (1985) (B)	1976	1B76B	157.68[b]	7.85	0.940
1BC	This Work	1976	1B76C	197.9(9)[b]	8.7(3)	0.93(1)
1NM64-N1	This Work	1976	1N76A	189.6(5)[b]	9.2(2)	0.926(9)
1NM64-N2	This Work	1976	1N76B	192.0(7)[b]	9.4(3)	0.94(1)
1NM64-N1	Caballero-Lopez and Moraal (2012)	1976	1N76C	8.6806	8.953	0.916
1NM64-N1	Stoker (1985)	1976	1N76D	151.67[b]	8.41	0.894
2BC	Dorman et al. (2000)	1996	2B96	—	9.694(37)	0.9954(38)
3NM64	Dorman et al. (2000)	1996	3N96	—	10.275(23)	0.9615(21)

[a]Figure in parenthesis is the 1σ uncertainty on the last decimal. Uncertainties were not provided for the previously published values. [b]Scaled units (not s^{-1}).

ilar solar modulation conditions. The solar modulation parameters calculated from Usoskin et al. (2017) were ~514 and ~518 MV, respectively, for the 1976 survey and 1995 survey. Averaged over the survey, the McMurdo neutron monitor count rates were within 2% of each other, and both surveys took place in epochs of positive solar magnetic polarity. Therefore, we compare the results directly, without any adjustment for changed modulation. Figure 9a illustrates leaded neutron monitor DRFs. (The 3NM64 DRF for 1995 from Nuntiyakul et al. (2014) is not shown here because it is indistinguishable from the one determined in this paper.) Two different designs of leaded monitors were used in 1976, denoted N1 and N2 in Table 4. We show four interpretations of the 1976 data. The first two result from applying our Dorman fit procedure to the summary data for N1 and N2 in Table 4 of Potgieter et al. (1980). We also show interpretations by Caballero-Lopez and Moraal (2012) and from the caption of Figure 1 of Stoker (1985). Because of various normalizations of the data the values of the parameter N_0 cannot be compared directly. The DRF for the 1996 survey uses the preferred Dorman functions from Dorman et al. (2000). We assume here that we can compare directly the DRF without solar modulation correction. Indeed, the 1996 survey was realized from December 1996 to March 1997 with an average solar modulation of 504 MV (calculated from updated parameters from Usoskin et al., 2017). This is very similar to the above-mentioned values for the 1976 and 1995 surveys.

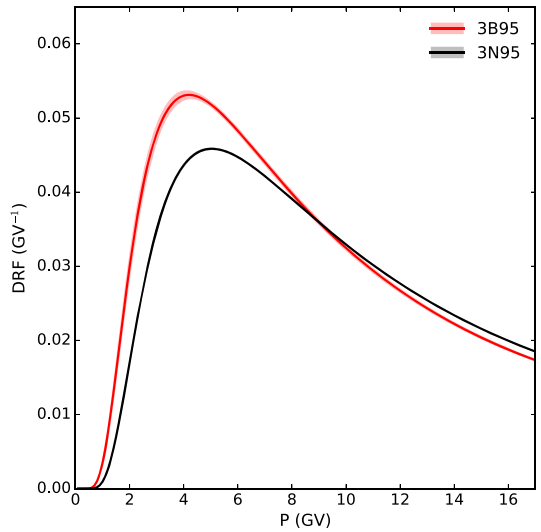

Figure 8. Comparison of the normalized differential response functions (bare neutron detectors and standard 3NM64) for the 1995 latitude survey.

The different interpretations of the 1976 NM64 data are all rather consistent, but all show a slightly higher response at low rigidity than the 1995 data. There is no evidence that this difference might be due to different primary spectra but it is possible that it represents a difference due to the use of 1NM64 detectors (of two slightly different designs) in the 1976 survey whereas the 1995 survey used a 3NM64. It is well known that the "outer" detectors in a multi-detector NM64 show a significantly lower count rate than the inner ones as they are, in effect, surrounded by less lead (Mangeard, Ruffolo, Sáiz & Madlee et al., 2016). In our survey, the average end-to-center ratio was 0.891. Based on a simple fit, it decreased by 0.002 from 0 to 16 GV cutoff, a result different from zero by slightly more that one standard deviation. We were able to reprocess simulations from a recent paper by Mangeard, Ruffolo, Sáiz and Nuntiyakul et al. (2016) to make a specific prediction of these quantities. The end-to-center ratio is reproduced to within 1%, with a predicted decline of 0.0032. We therefore think it is at least plausible that the 1NM64 may have slightly "softer" response function than a 3NM64. This is of interest to us in a practical sense, since the installation at South Pole is in fact three 1NM64 units, individually insulated and heated, but mounted on a common platform. We are currently running more detailed simulations to investigate the effect of this configuration at South Pole.

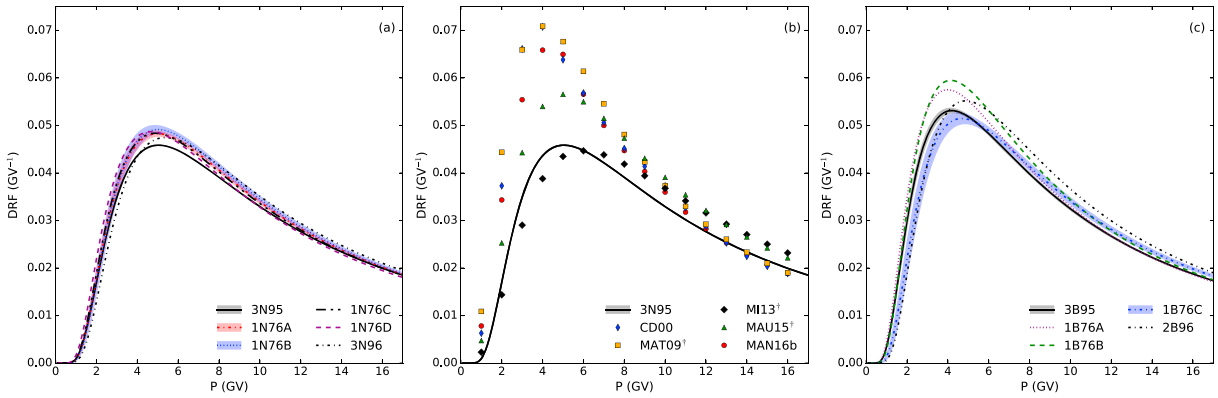

Figure 9. (a) Comparison of leaded neutron monitor response functions determined on latitude surveys. (b) Calculated response functions compared with the 1995 survey result. See text for details of this calculation. (c) Comparison of bare neutron detector response functions. Nomenclature for different surveys is defined in Table 4.

Figure 9b compares the observed normalized DRF of the 3NM64 of 1995 latitude survey with several calculations using recent computed models of "yield functions" (count rates as a function of rigidity and type of the primary particle at the top of the atmosphere). We used the model of Galactic cosmic ray spectra based on the local interstellar spectra (LIS) of proton and helium as proposed by Ghelfi et al. (2016), Ghelfi and Barao et al. (2017) and the force-field model of solar modulation from Gleeson and Axford (1968). For the period of the survey, the modulation parameter corresponding to this LIS was determined using the method presented in Ghelfi and Maurin et al. (2017) and was about 580 MV (the value was extracted from the database http://lpsc.in2p3.fr/crdb). Note that this is preferred for this purpose but it is different from the Usoskin et al. (2017) parameters used elsewhere in this paper. The nomenclature for the five simulated yield functions used in this work is as follows: CD00 from Clem and Dorman (2000), MAT09 from Matthiä et al. (2009), MI13 from Mishev et al. (2013), MAU15 from Maurin et al. (2015), and MAN16b from Mangeard, Ruffolo, Sáiz and Nuntiyakul et al. (2016). For MAT09 and MI13, the parametrizations of Maurin et al. (2015) were used (marked with a dagger in the Figure's legend). The differences between simulations are clearly visible with an overall agreement within 50%. Below 10 GV, MI13 provides a better estimate of the normalized DRF than the other models. Above 10 GV, the simulated results CD00, MAT09, and MAN16b provide a better estimate. More details about comparison between simulated yields can be found in Maurin et al. (2015) and Caballero-Lopez (2016).

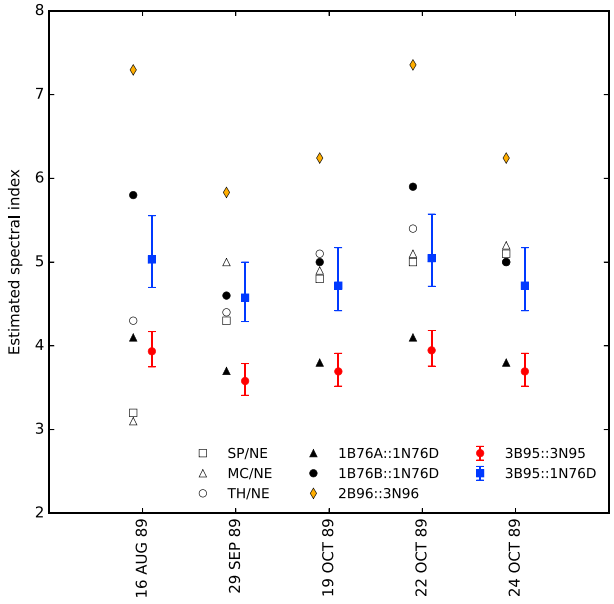

Figure 10. Comparison of estimated spectral indexes for GLEs of 1989. Black markers are taken unchanged from Bieber and Evenson (1991). Estimated spectral indices calculated in this article are shown in colored markers with error bars. Nomenclature for different surveys is defined in Table 4. More details are available in the text.

Figure 9(c) compares determinations of the BC response. Our result for 1995 agrees reasonably well with our analysis of the raw data for 1976 tabulated by Potgieter et al. (1980). What is rather surprising is the difference from the interpretation of Stoker (1985), where the "A" and "B" analyses were presented as an envelope of all possible fits to the data. At present, we have no specific comment on this apparent discrepancy. However as we have used the Stoker (1985) "B" results extensively in our previous work to use the BC/NM count rate ratio at South Pole to infer the spectral index of relativistic solar particles (Bieber & Evenson, 1991; Bieber et al., 2002, 2013; Sáiz et al., 2008), we have examined the extent to which this difference might influence our previous conclusions. Figure 10 is based on Figure 1 of Bieber and Evenson (1991), which compared spectral indices determined from NM64s at different P_c with the same events analyzed using the monitors and bare counters at South Pole alone. In this analysis, based on ratios of count rate increases, the implicit assumption is that the entire DRF scales with altitude with the same barometer coefficient—in other words, the entire altitude dependence may be expressed as a variation in N_0.

In Figure 10 the black symbols are taken directly from Bieber and Evenson (1991), where the open symbols are derived from station ratios (SP: South Pole, MC: McMurdo, TH: Thule, and NE: Newark) and the closed symbols from BC/NM ratios. The conclusion of that paper was that the "Stoker B"

interpretation of the BC/NM ratio at South Pole provided a better consistency with fixed station ratios, which was supported by comparison with the results of Cramp et al. (1997) as reported by Ruffolo et al. (2006). Applying this approach to the present work results in the red points. Here the error bars are constructed from the extremes allowed by the one sigma errors on the Dorman parameters discussed earlier. The result is similar to the "Stoker A" analysis, but like that analysis is not consistent with the station ratio determination. On the other hand, keeping in mind that the South Pole installation is actually three 1NM64 units we also show the result (blue symbols) obtained with the 1995 bare survey and the 1976 1NM64 result. Here the agreement with the station ratios is as good as that obtained with the "Stoker B" analysis.

In Figures 9 and 10 we also show the results from applying the Dorman et al. (2000) response functions, which are significantly different, presumably because the bare detectors in that work had no moderators.

5. Conclusions

We report an analysis of data taken using three bare neutron counters with a novel design and a standard three-counter neutron monitor (3NM64) on board the U.S. Coast Guard icebreaker *Polar Star* from 6 November 1995 to 20 March 1996, over a route from San Diego, USA, to McMurdo Base, Antarctica, and back to the northern Pacific Ocean. This latitude survey sampled geomagnetic cutoffs over $0 < P_c < 15$ GV, allowing a determination of the BC and 3NM64 response functions over that range. Various techniques were used to clean and correct the data. The pressure correction coefficient as a function of P_c was previously determined for this ship-borne 3NM64 (using data from 13 latitude surveys over 1994–2007), and here we investigated whether the BC count rate requires a different pressure coefficient. We concluded that the statistics available for these BCs are insufficient to determine whether the pressure coefficients are different, and therefore we used the same coefficient. The temperatures of both detector systems were controlled to some extent and we did not find a significant temperature effect on the count rates. The BC response was strongly affected by proximity to any port along the route, and such time periods were excluded when determining the response functions.

The only directly comparable latitude survey with bare neutron counters (of a different design, but with moderators) was performed in 1976 (Potgieter et al., 1980; Stoker et al., 1980), a time when solar modulation conditions were very similar to those in 1995. The neutron monitor response functions were similar, with small differences that might be attributed to the use of different pressure coefficients or the different detector design (1NM64 in 1976 versus 3NM64 in 1995). We will further investigate this effect for interpretation of data from the South Pole NM, which actually consists of three independent 1NM64 units. The BC response function for 1995 is similar to what we derive from the raw data from 1976 using the same analysis techniques but is substantially outside the allowed range according to Stoker (1985). One of the extremes of that range has been successfully used to determine the spectral index of relativistic solar particles from BC and NM data at South Pole during ground level enhancements. When applied in simplest form the results from the present work do not directly give such good agreement.

It must however be noted that the counting rates for the typically steep solar particle spectra at the high altitude of South Pole are determined in large part by response functions (or more properly the underlying yield functions) in a rigidity range below the atmospheric cutoff at sea level. Thus, the use of data from sea level surveys in this range is an extrapolation.

As the spectrum gets steeper the sensitivity to the choice of fit parameters also increases. In Figure 10 the formal errors on the spectral index for the apparently better choice of the parameters (blue points) are much larger than the formal errors on the less favored choice of parameters (red points) that would imply a flatter spectrum. In fact, the interpretation of the "Stoker A" and "Stoker B" as defining the range of variation in the spectral index allowed by uncertainties in the measured response is essentially confirmed. The BC to monitor comparison indeed gives a rather precise measurement of the spectral index, and in particular the variation of the spectral index within a given event (Ruffolo et al., 2006), but the actual value of the spectral index cannot be determined from latitude survey data alone.

In work in progress, we will follow up on this issue by analyzing data from a third latitude survey with BCs (of yet another design, but now installed at South Pole) conducted in 2009. We are investigating these various aspects of the analysis with Monte Carlo simulations, also currently in progress.

Acknowledgments
This study is supported in part by the Thailand Research Fund via grant RTA5980003 and Research Grant for New Scholar MRG6080086; by the U.S. National Science Foundation via awards PLR-1341562, PLR-1245939, and their predecessors; and by the Australian Antarctic Division. We thank the officers and crew of the USCG icebreaker Polar Star for their assistance in conducting the survey. We also thank Leonard Shulman, James Roth, and Keith Bolton for their technical assistance in preparing and maintaining the TasVan. W. N. would like to thank the Faculty of Science, Chandrakasem Rajabhat University, Bangkok, Thailand, for their support. The data displayed in the figures are available as supporting information.

References

Bieber, J. W., Clem, J., & Evenson, P. (1997). Efficient computation of apparent cutoffs. In *Proceedings of the 25th International Cosmic Ray Conference*, *2* (pp. 389–392). Transvaal, South Africa: Potchefstroom University.

Bieber, J. W., Clem, J., Evenson, P., Pyle, R., Sáiz, A., & Ruffolo, D. (2013). Giant ground level enhancement of relativistic solar protons on 2005 January 20. I. Spaceship Earth Observations. *Astrophysical Journal*, *771*, 92. https://doi.org/10.1088/0004-637X/771/2/92

Bieber, J. W., Dröge, W., Evenson, P., Pyle, R., Ruffolo, D., Pinsook, U., et al. (2002). Energetic particle observations during the 2000 July 14 solar event. *Astrophysical Journal*, *567*, 622–634. https://doi.org/10.1086/338246

Bieber, J. W., & Evenson, P. (1991). Determination of energy spectra for the large solar particle events of 1989. In *Proceedings of the 22nd International Cosmic Ray Conference* (Vol. 3, pp. 129–132). Dublin, Ireland.

Caballero-Lopez, R. A. (2016). An estimation of the yield and response functions for the mini neutron monitor. *Journal of Geophysical Research: Space Physics*, *121*, 7461–7469. https://doi.org/10.1002/2016JA022690

Caballero-Lopez, R. A., & Moraal, H. (2012). Cosmic-ray yield and response functions in the atmosphere. *Journal of Geophysical Research: Space Physics*, *117*, A12103. https://doi.org/10.1029/2012JA017794

Clem, J. M., Bieber, J. W., Evenson, P., Hall, D., Humble, J. E., & Duldig, M. (1997). Contribution of obliquely incident particles to neutron monitor counting rate. *Journal of Geophysical Research*, *102*, 26,919–26,926. https://doi.org/10.1029/97JA02366

Clem, J. M., & Dorman, L. I. (2000). Neutron monitor response functions. *Space Science Reviews*, *93*, 335–359. https://doi.org/10.1023/A:1026508915269

Cramp, J. L., Duldig, M. L., Flückiger, E. O., Humble, J. E., Shea, M. A., & Smart, D. F. (1997). The October 22, 1989, solar cosmic ray enhancement: An analysis of the anisotropy and spectral characteristics. *Journal of Geophysical Research*, *102*, 24,237–24,248. https://doi.org/10.1029/97JA01947

Dorman, L. I., Fedchenko, S. G., Granitsky, L. V., & Rishe, G. A. (1969). Coupling and barometer coefficients for measurements of cosmic ray variations at altitudes of 260–400 mb. In *Proceedings of the 11th International Conference on Cosmic Rays* (Vol. 2, pp. 233–236). Budapest.

Dorman, L. I., Villoresi, G., Iucci, N., Parisi, M., Tyasto, M. I., Danilova, O. A., & Ptitsyna, N. G. (2000). Cosmic ray survey to Antarctica and coupling functions for neutron component near solar minimum (1996–1997): 3. Geomagnetic effects and coupling functions. *Journal of Geophysical Research: Space Physics*, *105*, 21,047–21,056. https://doi.org/10.1029/2000JA900051

Evenson, P., Bieber, J. W., Clem, J., & Pyle, R. (2005). Neutron monitor temperature coefficients: Measurements for BF_3 and ^{3}He counter tubes. In *Proceedings 29th International Cosmic Ray Conference* (Vol. 2, pp. 485–488). Pune, India.

Ghelfi, A., Barao, F., Derome, L., & Maurin, D. (2016). Non-parametric determination of H and He interstellar fluxes from cosmic-ray data. *Astronomy and Astrophysics*, *591*, A94. https://doi.org/10.1051/0004-6361/201527852

Ghelfi, A., Barao, F., Derome, L., & Maurin, D. (2017). Non-parametric determination of H and He interstellar fluxes from cosmic-ray data (Corrigendum). *Astronomy and Astrophysics*, *605*, C2. https://doi.org/10.1051/0004-6361/201527852e

Ghelfi, A., Maurin, D., Cheminet, A., Derome, L., Hubert, G., & Melot, F. (2017). Neutron monitors and muon detectors for solar modulation studies: 2. ϕ time series. *Advances in Space Research*, *60*, 833–847. https://doi.org/10.1016/j.asr.2016.06.027

Gleeson, L. J., & Axford, W. I. (1968). Solar modulation of galactic cosmic rays. *Astrophysical Journal*, *154*, 1011–1026. https://doi.org/10.1086/149822

Hatton, C. J., & Carmichael, H. (1964). Experimental investigation of the NM-64 neutron monitor. *Canadian Journal of Physics*, *42*, 2443–2472. https://doi.org/10.1139/p64-222

Kouzes, R. T., Siciliano, E. R., Ely, J. H., Keller, P. E., & McConn, R. J. (2008). Passive neutron detection for interdiction of nuclear material at borders. *Nuclear Instruments and Methods in Physics Research Section A: Accelerators, Spectrometers, Detectors and Associated Equipment*, *584*, 383–400. https://doi.org/10.1016/j.nima.2007.10.026

Lin, Z., Bieber, J. W., & Evenson, P. (1995). Electron trajectories in a model magnetosphere: Simulation and observation under active conditions. *Journal of Geophysical Research*, *100*, 23,543–23,549. https://doi.org/10.1029/95JA02696

Mangeard, P.-S., Ruffolo, D., Sáiz, A., Madlee, S., & Nutaro, T. (2016). Monte Carlo simulation of the neutron monitor yield function. *Journal of Geophysical Research: Space Physics*, *121*, 7435–7448. https://doi.org/10.1002/2016JA022638

Mangeard, P.-S., Ruffolo, D., Sáiz, A., Nuntiyakul, W., Bieber, J. W., Clem, J., et al. (2016). Dependence of the neutron monitor count rate and time delay distribution on the rigidity spectrum of primary cosmic rays. *Journal of Geophysical Research: Space Physics*, *121*, 11,620–11,636. https://doi.org/10.1002/2016JA023515

Matthiä, D., Heber, B., Reitz, G., Meier, M., Sihver, L., Berger, T., & Herbst, K. (2009). Temporal and spatial evolution of the solar energetic particle event on 20 January 2005 and resulting radiation doses in aviation. *Journal of Geophysical Research*, *114*, A08104. https://doi.org/10.1029/2009JA014125

Maurin, D., Cheminet, A., Derome, L., Ghelfi, A., & Hubert, G. (2015). Neutron monitors and muon detectors for solar modulation studies: Interstellar flux, yield function, and assessment of critical parameters in count rate calculations. *Advances in Space Research*, *55*, 363–389. https://doi.org/10.1016/j.asr.2014.06.021

Mishev, A. L., Usoskin, I. G., & Kovaltsov, G. A. (2013). Neutron monitor yield function: New improved computations. *Journal of Geophysical Research: Space Physics*, *118*, 2783–2788. https://doi.org/10.1002/jgra.50325

Muangha, P. (2013). *Observation of Cosmic Ray Apectral Variation Using Bare Counters at Doi Inthanon with Princess Sirindhorn Neutron Monitor, Unpublished Undergraduate Senior Project*. Bangkok, Thailand: Mahidol University.

Nuntiyakul, W., Evenson, P., Ruffolo, D., Sáiz, A., Bieber, J. W., Clem, J., et al. (2014). Latitude survey investigation of Galactic cosmic ray solar modulation during 1994–2007. *Astrophysical Journal*, *795*, 11. https://doi.org/10.1088/0004-637X/795/1/11

Potgieter, M. S., Raubenheimer, B. C., Stoker, P. H., & van der Walt, A. J. (1980). Modulation of cosmic rays during solar minimum. Part 2. Cosmic ray latitude distribution at sea-level during 1976. *South African Journal of Physics*, *3*(3–4), 77–89.

Ruffolo, D., Sáiz, A., Mangeard, P.-S., Kamyan, N., Muangha, P., Nutaro, T., et al. (2016). Monitoring short-term cosmic-ray spectral variations using neutron monitor time-delay measurements. *Astrophysical Journal*, *817*(38). https://doi.org/10.3847/0004-637X/817/1/38

Ruffolo, D., Tooprakai, P., Rujiwarodom, M., Khumlumlert, T., Wechakama, M., Bieber, J. W., et al. (2006). Relativistic solar protons on 1989 October 22: Injection and transport along both legs of a closed interplanetary magnetic loop. *Astrophysical Journal*, *639*, 1186–1205. https://doi.org/10.1086/499419

Sáiz, A., Ruffolo, D., Bieber, J. W., Evenson, P., & Pyle, R. (2008). Anisotropy signatures of solar energetic particle transport in a closed interplanetary magnetic loop. *Astrophysical Journal*, *672*, 650–658. https://doi.org/10.1086/523663

Simpson, J. A. Jr. (1948). The latitude dependence of neutron densities in the atmosphere as a function of altitude. *Physical Review*, *73*, 1389–1391. https://doi.org/10.1103/PhysRev.73.1389

Stoker, P. H. (1985). Spectra of solar proton ground level events using neutron monitor and neutron moderated detector recordings. In *Proceedings 19th International Cosmic Ray Conference* (Vol. 4, pp. 114–117).

Stoker, P. H., & Raubenheimer, B. C. (1985). The neutron moderated detector and groundbased cosmic ray modulation studies. In *Proceedings 19th International Cosmic Ray Conference* (Vol. 5, pp. 502–505).

Stoker, P. H., van der Walt, A. J., & Potgieter, M. S. (1980). Modulation of cosmic rays during solar minimum. Part 1. Cosmic ray intensity survey at sea-level during 1976: Experimental details. *South African Journal of Physics*, *3*, 73–76.

Thomsen, M. F. (2004). Why K_p is such a good measure of magnetospheric convection. *Space Weather*, *2*, S11004. https://doi.org/10.1029/2004SW000089

Tsyganenko, N. A. (1987). Global quantitative models of the geomagnetic field in the cislunar magnetosphere for different disturbance levels. *Planetary and Space Science*, *35*, 1347–1358. https://doi.org/10.1016/0032-0633(87)90046-8

Usoskin, I. G., Gil, A., Kovaltsov, G. A., Mishev, A. L., & Mikhailov, V. V. (2017). Heliospheric modulation of cosmic rays during the neutron monitor era: Calibration using PAMELA data for 2006–2010. *Journal of Geophysical Research: Space Physics*, *122*, 3875–3887. https://doi.org/10.1002/2016JA023819

Villoresi, G., Dorman, L. I., Iucci, N., & Ptitsyna, N. G. (2000). Cosmic ray survey to Antarctica and coupling functions for neutron component near solar minimum (1996–1997): 1. Methodology and data quality assurance. *Journal of Geophysical Research*, *105*, 21,025–21,034. https://doi.org/10.1029/2000JA900048

Zreda, M., Desilets, D., Ferré, T. P. A., & Scott, R. L. (2008). Measuring soil moisture content non-invasively at intermediate spatial scale using cosmic-ray neutrons. *Geophysical Research Letters*, *35*, L21402. https://doi.org/10.1029/2008GL035655